

# Regime dependent changes in global precipitation

Richard P. Allan

Received: 19 April 2011 / Accepted: 20 June 2011 / Published online: 8 July 2011  
© Springer-Verlag 2011

**Abstract** Assessment of changes in precipitation ( $P$ ) as a function of percentiles of surface temperature ( $T$ ) and 500 hPa vertical velocity ( $\omega$ ) are presented, considering present-day simulations and observational estimates from the Global Precipitation Climatology Project (GPCP) combined with the European Centre for Medium-range Weather Forecasts Interim reanalysis (ERA Interim). There is a tendency for models to overestimate  $P$  in the warm, subsiding regimes compared to GPCP, in some cases by more than 100%, while many models underestimate  $P$  in the moderate temperature regimes. Considering climate change projections between 1980–1999 and 2080–2099, responses in  $P$  are characterised by  $dP/dT \geq 4\%/K$  over the coldest 10–20% of land points and over warm, ascending ocean points while  $P$  declines over the warmest, descending regimes ( $dP/dT \sim -4\%/K$  for model ensemble means). The reduced Walker circulation limits this contrasting  $dP/dT$  response in the tropical wet and dry regimes only marginally. Around 70% of the global surface area exhibits a consistent sign for  $dP/dT$  in at least 6 out of a 7-member model ensemble when considering  $P$  composites in terms of dynamic regime.

**Keywords** Precipitation · Climate models · Dynamical regime

## 1 Introduction

Predicting regional changes in precipitation over the coming decades is of great importance to societies yet remains a considerable scientific challenge. However, robust responses in the hydrological cycle are emerging at the large scale (Mitchell et al. 1987; Held and Soden 2006):

- (1) global precipitation increases in response to the enhanced atmospheric radiative cooling to the surface in a warmer climate (Allen and Ingram 2002; Stephens and Ellis 2008; Lambert and Webb 2008) at around 1–3%/K,
- (2) large-scale precipitation events are dependent on moisture convergence (Trenberth et al. 2003) which enhances in proportion to low-level water vapour increases of around 6–7%/K (O’Gorman and Muller 2010; Willett et al. 2008),
- (3) enhanced moisture transport from the dry moisture source regions to the moist tropics and mid-latitude storm track regions (Held and Soden 2006) contributes to a drying of the already dry sub-tropical regions (Chou et al. 2007; Allan et al. 2010).

Regionally the above large-scale driving mechanisms may all contribute to a particular location during different months depending on the position of the large-scale atmospheric circulation. It is therefore difficult both to detect and project regional changes in precipitation which are strongly dependent upon large-scale circulation patterns (Pal et al. 2004).

The aim of the present study is to introduce a technique for understanding changes in precipitation that are independent of local changes in circulation. Numerous studies have shown the value of analysing cloud and precipitation as a function of vertical motion (e.g. Bony et al. 2004;

---

R. P. Allan (✉)  
Department of Meteorology, National Centre for Atmospheric  
Science (NCAS)—Climate, University of Reading,  
Reading, Berkshire, UK  
e-mail: r.p.allan@reading.ac.uk

Emori and Brown 2005; Chou et al. 2009; Williams and Ringer 2010). While precipitation ( $P$ ) is directly tied to vertical motion,  $P$  is also related to the amount of moisture available for condensation which is linked, through the Clausius Clapeyron equation, to surface temperature ( $T$ ). The radiative constraint upon  $P$  is also strongly tied to  $T$  (Mitchell et al. 1987; Andrews et al. 2010). This motivates the use of temperature as a variable for understanding precipitation changes in addition to vertical motion.

Regional changes in precipitation are difficult to understand physically (Chou et al. 2009), despite some recent advances (Xie et al. 2010). Therefore the aim of the present study is to extract the robust, physically understandable component of precipitation changes, extending recent advances (Emori and Brown 2005; Chou et al. 2009) by considering changes in precipitation in distinct regimes characterised by the overall distribution of temperature and vertical motion. Gridded global, monthly precipitation data is composited into bins of surface temperature ( $T$ ) and vertical motion ( $\omega$ ), thereby sampling distinct dynamical regimes (for example the warm, ascending branch of the tropical circulation) and seeking process-based responses that are independent of location. Separation of the  $P$  responses distinct from the influences of local changes in large-scale circulation is a potentially useful method for improving understanding of current and future changes in the global water cycle (Emori and Brown 2005). In the current study we focus on the methodology, comparisons between observational estimates of precipitation and present day model simulations and contrast these with climate change projections.

## 2 Data and methodology

Climate model simulations of the present day are compared with observational estimates and simulations of future

changes. Monthly mean precipitation is composited into bins ranging from the coolest to the warmest temperatures and from the strongest descent to the strongest ascent. In doing so attempt is made to understand the regime-dependent changes in precipitation.

### 2.1 Model data

Ten climate models submitted to the 3rd Coupled Model Intercomparison Project (CMIP3; Meehl et al. 2007b) are considered (Table 1). For each model 3 experiments were chosen: (1) AMIP: atmosphere only simulations (1980–1999) forced with the observed estimates of sea surface temperature and sea ice fields, (2) 20C3: 20th Century coupled model simulations (1980–1999) with realistic changes in radiative forcing, (3) SRESA1B: simulations of future climate change using the SRES A1B scenario for 2080–2099. Monthly mean precipitation ( $P$ ), vertical pressure velocity at 500 hPa ( $\omega$ ) and surface temperature ( $T$ ) were analysed. These models provide a sample of physically plausible climate simulations and were chosen due to the availability of all experiments and diagnostics required. Therefore it is important to highlight that this set of models do not cover the overall uncertainty in climate change responses and are merely an ensemble of opportunity.

### 2.2 Observations

Observational estimates of  $P$  were taken from the Global Precipitation Climatology Project (GPCP) version 2.1 (Huffman et al. 2009). These estimates combine infra-red radiances with microwave retrievals over ocean and rain-gauge data over land. The record prior to August 1987 does not include satellite microwave data. Here, analysis of GPCP data is restricted to the period after 1988. Observational estimates of surface  $T$  and 500 hPa  $\omega$  were taken from the European Centre for Medium Range Weather Forecasts Interim reanalysis (ERA Interim; Dee et al.

**Table 1** CMIP3 climate models

Model	Description	Reference
<i>cnrm_cm3</i>	Centre National de Recherches Meteorologiques CM3 model, France	Salas-Méla et al. (2005)
<i>giss_model_er</i>	Goddard Institute for Space Studies Model ER, USA	Schmidt et al. (2006)
<i>iap_fggoals1_0_g</i>	National Key Laboratory of Numerical Modeling for Atmospheric Sciences, China	Yu et al. (2004)
<i>inmcm3_0</i>	Institute for Numerical Mathematics, CM3 model, Russia	Volodin and Diansky (2004)
<i>ipsl_cm4</i>	Institut Pierre Simon Laplace, CM4 model, France	Marti et al. (2005)
<i>miroc3_2_hires</i>	Center for Climate System Research, high resolution version, Japan	Hasumi and Emori (2004)
<i>miroc3_2_medres</i>	Center for Climate System Research, medium resolution version, Japan	Hasumi and Emori (2004)
<i>mri_cgcm2_3_2a</i>	Meteorological Research institute CGCM2 model, Japan	Yukimoto and Noda (2002)
<i>ncar_ccsm3_0</i>	National Center for Atmospheric Research, CCSM3 model, USA	Collins et al. (2006)
<i>ukmo_hadgem1</i>	Met Office Hadley Centre Global Environment Model version 1, UK	Johns et al. (2006)

(2011)). For comparison with the model simulations of the present day we consider the period 1989–1999.

### 2.3 Compositing precipitation by vertical motion and surface temperature

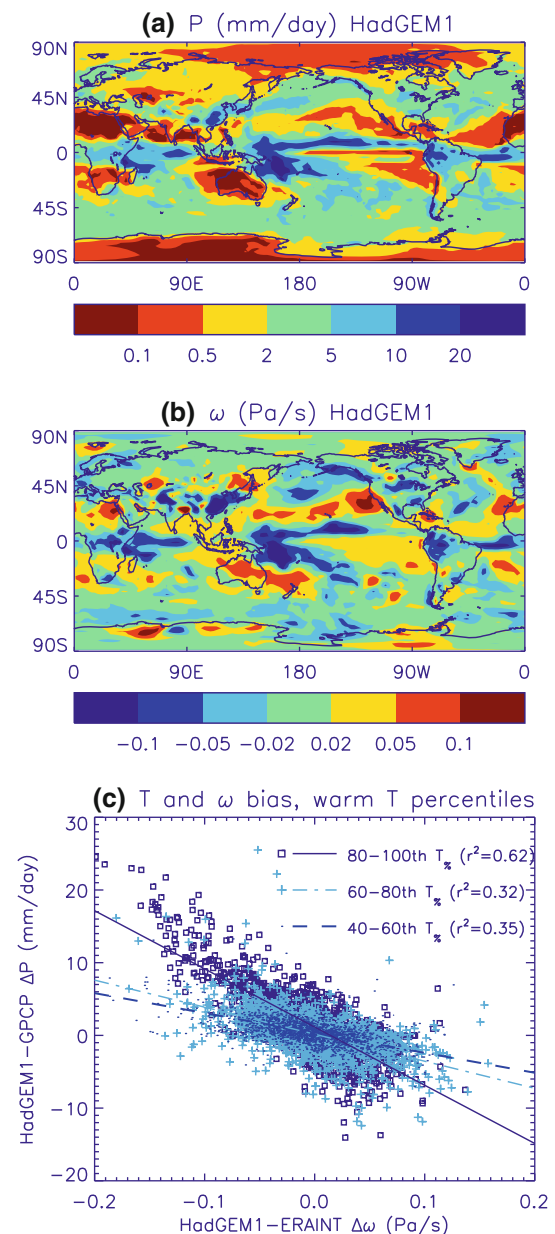
Globally, changes in the atmospheric and surface radiative energy balance dictate the responses in global mean  $P$  (Andrews et al. 2010; Allan 2009) and these are linked with surface  $T$  changes through relatively minor changes in  $T$  lapse rate and relative humidity (e.g. Lambert and Webb 2008). Locally, the relationship between  $P$  and surface  $T$  is more complex, particularly over land where cause and effect are difficult to establish (Trenberth and Shea 2005) and where responses in vertical motion to local  $T$  or external drivers are important.

The relationship between 500 hPa vertical motion and  $P$  is demonstrated in Fig. 1 for the HadGEM1 model AMIP simulation for April 1995 as an example of the methodology employed in the present study. There is a close relationship between  $P$  (Fig. 1a) and  $\omega$  (Fig. 1b) in low latitudes with negative  $\omega$  (ascending motion) corresponding with larger  $P$ . The relationship between model bias in  $P$  and  $\omega$  is strongest for the 20% (by area) warmest grid boxes (Fig. 1c) with 62% of the variance in  $P$  bias explained by bias in  $\omega$ . The weakest  $P - \omega$  relationship is found for the coldest 20% of grid boxes (not shown) where less than 10% of the variance is explained.

The strong relationships locally between  $P$ , surface  $T$  and  $\omega$  motivate the strategy employed in the following sections which is to composite  $P$  in terms of the two primary driving variables, surface  $T$  and vertical motion,  $\omega$ . An example is illustrated in Fig. 2 for the HadGEM1 AMIP simulation and GPCP data for April 1995.

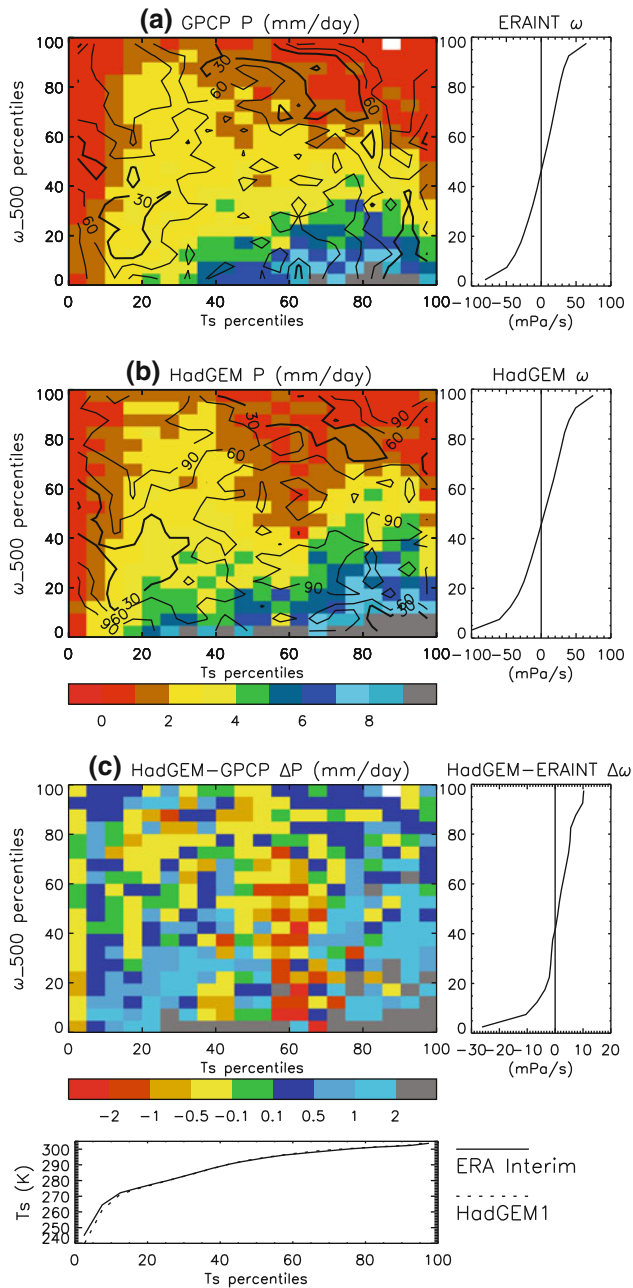
In the following analysis, each global monthly field was re-gridded to the regular  $2.5 \times 2.5$  degree latitude-longitude GPCP grid using bi-linear interpolation. Area weighted histograms of the global  $T$  and  $\omega$  fields were computed and bin boundaries determined every 5 percentiles of the distribution (from the coldest bins to the warmest bins and from the strongest ascent to the strongest descent). Monthly gridded  $P$  values were then composited by each of the 20  $T$  and 20  $\omega$  percentile bins (400 bin boxes in total).

Figure 2 shows the resulting two dimensional  $P$  composite for April 1995 as a function of surface  $T$  and 500 hPa  $\omega$  bins for (a) GPCP data, (b) HadGEM1 simulations and (c) HadGEM1 minus GPCP. Also shown are percentile bin mean  $\omega$  (right panels) and surface  $T$  (bottom panel), demonstrating the progression from negative  $\omega$  (ascent) to positive  $\omega$  (descent) with increasing  $\omega$  percentiles, and the increase in surface  $T$  with percentile bin, the largest rate of rise occurring for the coldest  $T$  bins.



**Fig. 1** Monthly mean (a) precipitation (mm/day) and (b) vertical motion (Pa/s) simulated by HadGEM1 for April 1995 and (c) relationships between model bias in precipitation (HadGEM1-GPCP) and vertical motion (HadGEM1-ERA Interim) for the warmest percentiles of global temperature (40–60th, 60–80th and 80–100th percentiles)

The observed and simulated  $P$  distributions show maxima for the highest (warmest)  $T$  percentile bins and lowest  $\omega$ -percentile bins (strongest ascending motion) as expected from Fig. 1. The lowest  $P$  values are found in the strongest descent bins ( $\geq 80$ th percentile of  $\omega$ ) and the coldest 5% of  $T$  grid points. There are however moderate  $P$  totals for the strongest descent ( $>80$ th percentile of  $\omega$ ) for 20–40th  $T$  percentiles, corresponding to mid-latitude ocean regions, where  $\omega$  at 500 hPa is not such a good proxy for precipitation.



**Fig. 2** Mean precipitation (colours) for April 1995 in percentile bins of vertical motion and temperature for **a** GPCP and ERA Interim, **b** HadGEM1 and **c** HadGEM1-GPCP. Contours in **a** and **b** indicate the percentage of data points enclosed. Also shown is the mean vertical motion as a function of vertical motion bin (right) and the mean surface temperature as a function of temperature bin (bottom)

Also shown in Fig. 2a and b are contours which enclose the area-weighted percentage of the globe sampled. The 60% contour encloses bin boxes that sample 60% of the global surface area and this samples the highest  $T$  and low  $\omega$  percentiles (warm, ascending region), high  $\omega$  and moderate  $T$  percentiles (strong descent and moderate

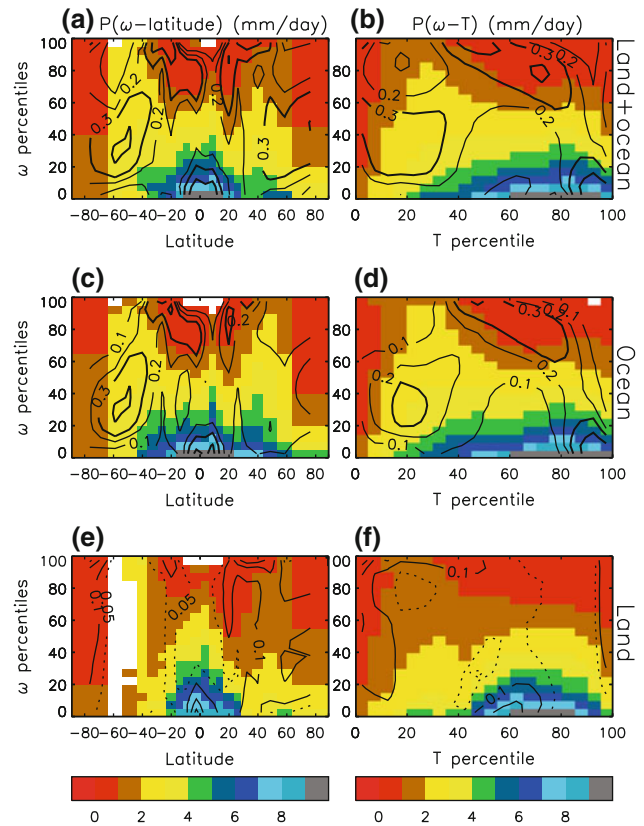


**Fig. 3** Mean GPCP precipitation (colour scale, mm/day) in percentile bins of ERA Interim 500 hPa vertical motion ( $\omega$ ) and either latitude bins (**a**, **c**, **e**) or percentile bins of ERA Interim surface temperature (**b**, **d**, **f**) for land and ocean (**a**, **b**), ocean only (**c**, **d**) and land only (**e**, **f**) for 1989–2008. Contours (at 0.05, 0.1, 0.2, 0.3 and 0.5%) show the contribution of each bin box expressed as a percentage of the global mean area. Mean  $P$  is displayed only where at least 30% of months contain valid values

temperatures) and the low  $T$  and low  $\omega$  percentiles (cold but ascending regimes).

Model minus GPCP  $P$  bias is displayed in Fig. 2c. There is an overestimate of  $>2$  mm/day for 65% of the 0–5 percentile  $\omega$  bin (strongest ascent). This is consistent with a model underestimate in the mean strength of ascending motion by around 25 mPa/s compared to ERA Interim. Although the bias field for a single month is noisy, there is a tendency for the model to overestimate  $P$  for regions of ascent ( $\omega < 0$ ) and to underestimate  $P$  for descending regimes ( $\omega > 0$ ), consistent with the overall bias in  $\omega$ . The main exception is a model negative  $P$  bias around the 60th  $T$  percentile (around 295 K) for ascending regions although this region does not contribute a large fraction of global coverage. The model simulates lower  $P$  than GPCP for the coldest bin (Antarctica) and also  $\sim 5$  K lower surface  $T$  than ERA Interim. It is not clear how reliable the GPCP

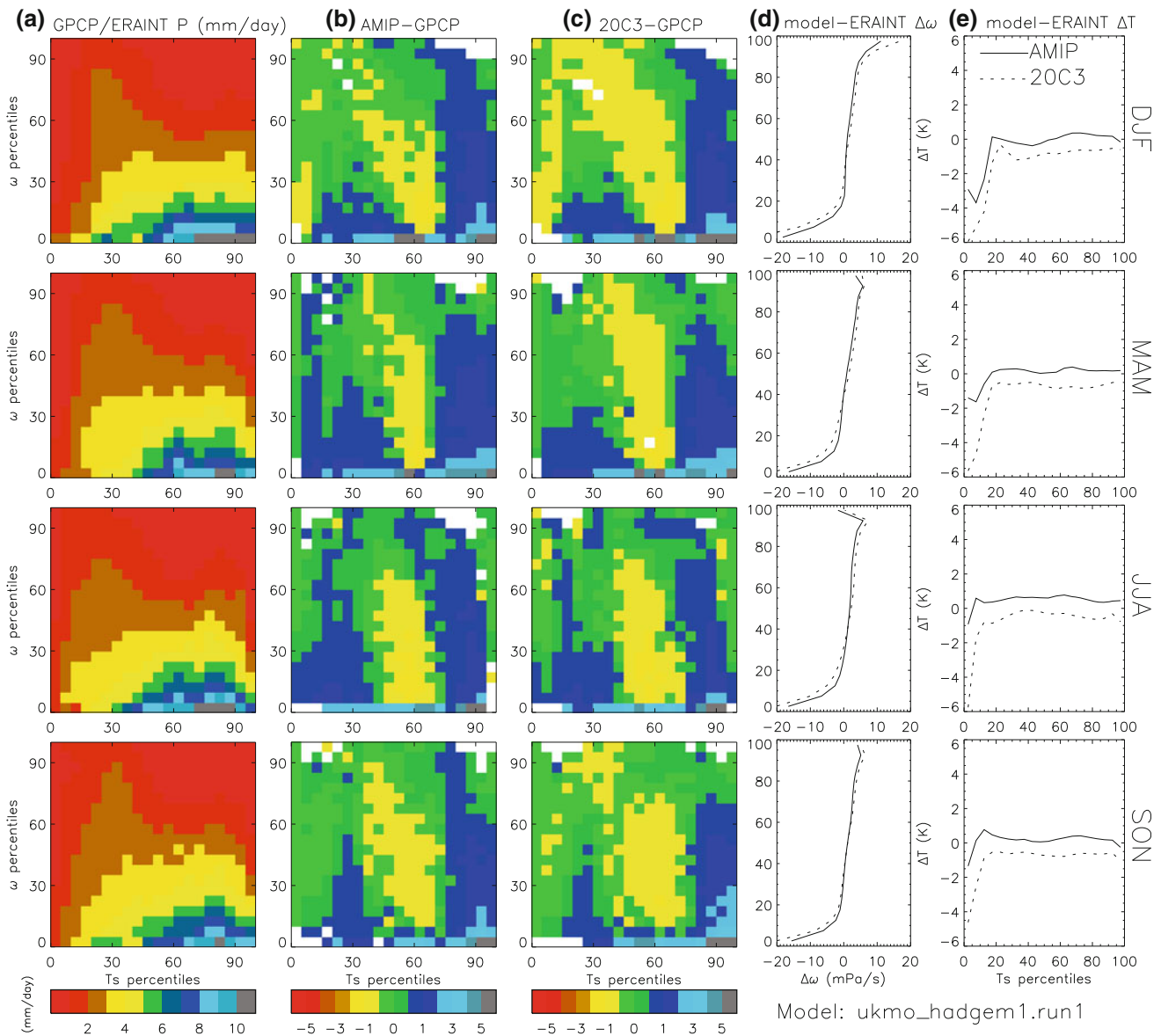


**Fig. 4** Observed GPCP seasonal mean binned precipitation (a) and model-GPCP precipitation differences for (b) AMIP and (c) 20C3 HadGEM1 experiments for 1989–1999. Model-ERA Interim vertical

motion and surface temperature differences are shown in columns d, e. For b, c, green denotes differences of  $\pm 0.2$  mm/day

and ERA Interim data are over this region in particular for a single month.

The  $P$  distributions may subsequently be composited over time to generate mean distributions globally and over land and ocean separately. Figure 3 shows the 1989–2008 GPCP  $P$  distributions in latitude bins and  $\omega$  percentile bins (left) and percentile bins of both  $T$  and  $\omega$  (right). Although  $T$  strongly depends upon latitude, binning by  $T - \omega$  generates a smoother  $P$  distribution and allows changes in  $P$  to be interpreted more clearly in terms of the physical driving variables. Hence, this method is preferred in the analysis of observed and simulated changes in  $P$ .

### 3 Simulation of present-day precipitation composites

Climate model simulations for the period 1989–1999 are now compared with observational estimates using the precipitation compositing technique described in Sect. 2. The sensitivity of this technique to season and simulation experiment is first assessed for the HadGEM1 model in Fig. 4.

#### 3.1 Seasonal composites

The observed joint distribution of  $P$  from GPCP (as a function of  $\omega$  and  $T$  percentiles from ERA Interim) is

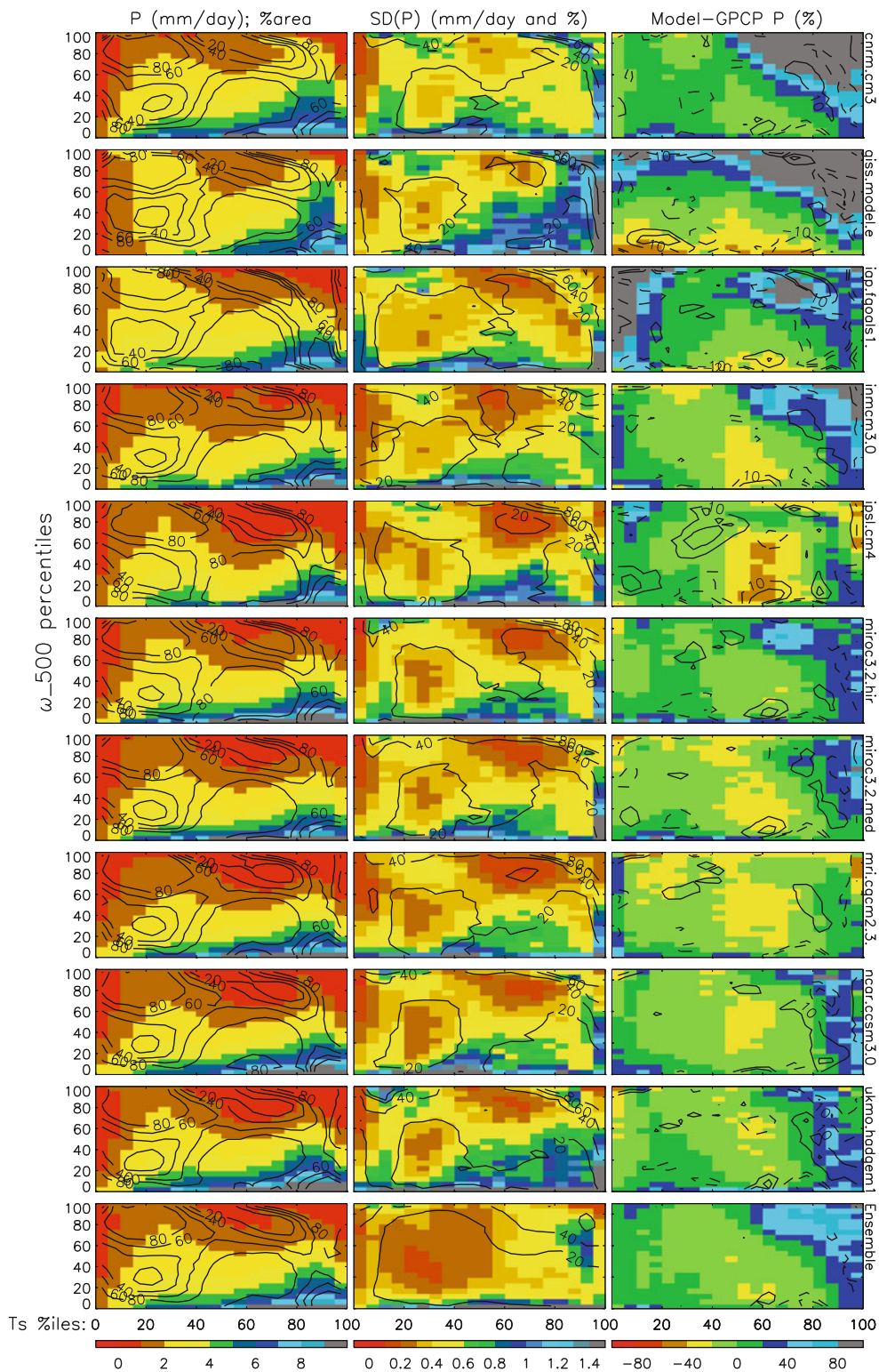


**Fig. 5** Multi-model (CMIP3) binned precipitation with contours denoting percentage (by area) of data-points enclosed (left), standard deviation of precipitation (middle) in mm/day (colours) and expressed as a percentage of mean  $P$  (contours) and model-GPCP precipitation as a percentage difference with contours showing differences in

percentage contribution to each bin box (right). The bottom row shows multi-model mean precipitation, its multi-model standard deviation and multi-model mean binned difference to GPCP/ERA Interim for the period 1989–1999

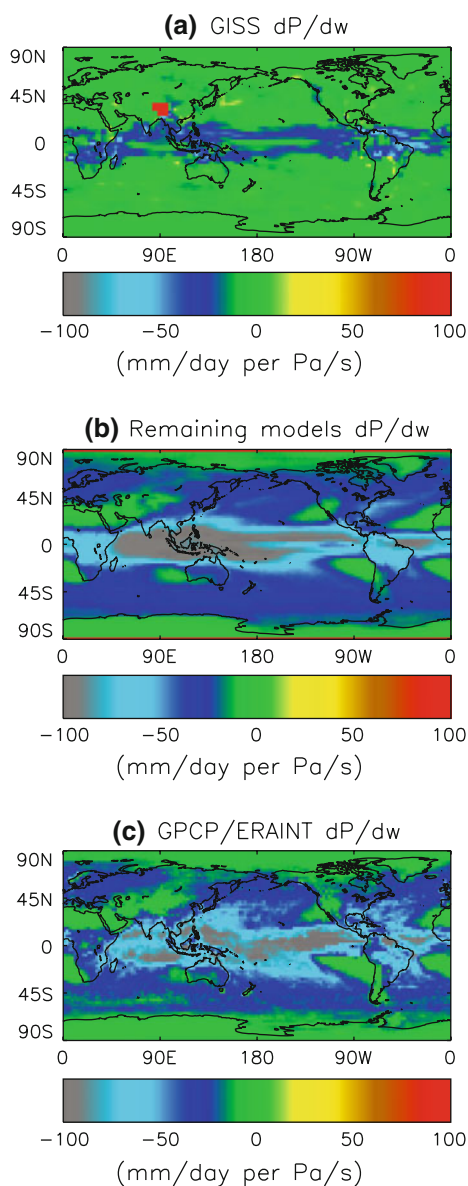


**Fig. 6** Estimated sensitivity of monthly precipitation to changes in 500 hPa vertical motion ( $dP/d\omega$ ) for (a) the GISS\_E\_R model, (b) a mean of the remaining models and (c) an observational estimate based upon GPCP and ERA Interim. A linear least squares fit was calculated separately for each season and each model and the resulting sensitivity  $dP/d\omega$  was averaged over the four seasons and over all models apart from GISS\_E\_R in (b)

relatively insensitive to season (Fig. 4a) and broadly consistent with the monthly example in Fig. 2a. This demonstrates that while the regional patterns of  $P$  vary from month to month, the distribution expressed as a function of  $T$  and  $\omega$  percentiles remains relatively robust as anticipated.

HadGEM1 minus GPCP differences in  $P$  also show consistent signals for each season and for the two distinct experiments, AMIP (Fig. 4b) and 20C3 (Fig. 4c). The

model simulates larger  $P$  compared to GPCP for the 0–5%  $\omega$  bin (strongest ascent) and this is consistent with a negative  $\omega$  bias (mean ascent is stronger by up to 20 *mPa/s* compared to ERA Interim). There is also a tendency for the model experiments to simulate greater  $P$  than GPCP ( $>0.2$  mm/day) for the warmer  $T$  percentiles ( $>70$ th percentile) and underestimate  $P$  by a similar magnitude for the 40–70th  $T$  percentiles.

The coldest  $T$  percentiles in the model simulations are colder than ERA Interim. While the AMIP experiment is constrained to agree with ice-free ocean temperature observations, the coupled experiment (20C3) simulates temperatures around 1 K cooler on average than ERA Interim for most  $T$  percentiles.

### 3.2 Multi-model annual composites

Multi-annual composites of  $P$  for a range of CMIP3 model 20C3 coupled experiments are compared in Fig. 5 for the period 1989–1999. Mean  $P$  is shown in the left column for each model and a multi-model ensemble mean (sum of the 10 composites) is displayed in the bottom row. Overlaid are contours enclosing the percentage of global area coverage (boxes within the 60% contour enclose 60% of the global area). The  $P$  composites and area enclosed again show a broadly consistent, but smoother, pattern compared to the April 1995 HadGEM1 composite: most of the data resides in the warmest ascending bins, moderately warm (50–80th  $T$  percentiles) descending bins (highest  $\omega$  percentiles) or the cool, weakly ascending bins (around 20th  $T$  percentile and 30th  $\omega$  percentile).

The standard deviation of precipitation ( $SD(P)$ ) within each bin box (over all 132 months) is displayed in the middle panel of Fig. 5 for each model. This is expressed in mm/day (colours) and also as a percentage of mean  $P$  (contours). The ensemble mean shows  $SD(P)$  across all 10 model means in each bin box rather than a mean of the model standard deviations (contours again show  $SD(P)$  expressed as a percentage of multi-model mean  $P$  for each bin box).

As expected the largest variation ( $SD(P) > 1$  mm/day) is for the lowest  $\omega$  percentiles (strongest ascent) where  $P$  is largest. However, there are also anomalously large  $SD(P)$  for the highest  $\omega$  and lowest  $T$  percentile bins for some models (e.g. HadGEM1). These regions do not contribute a significant fraction of the global area and may contain months without valid data (e.g. see Fig. 4). The GISS model also displays large  $SD(P)$  for the warmest  $T$  bins, generally representative of land grid boxes. In general the  $SD(P)$  is around 20% of mean  $P$  in each bin box. The exception is for the highest  $T$  and  $\omega$  bins (warm, dry, descending regimes) in which the  $SD(P)$  is above 60% of the mean  $P$  which is generally  $< 1$  mm/day.

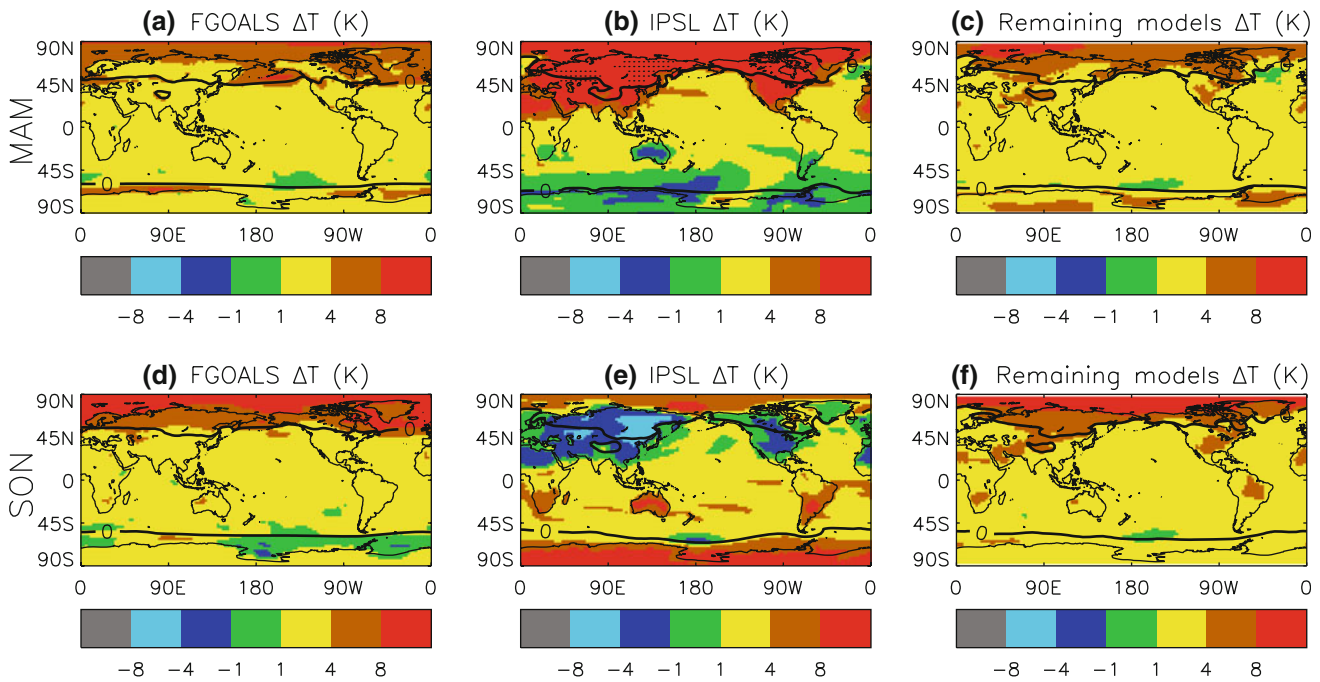


**Fig. 7** Changes in surface temperature for 2080–2099 minus 1980–1999 for MAM (top) and SON (bottom) for IOP FGOALS, IPSL and an ensemble of the remaining models. A contour of the

mean 0°C isotherm for 1980–1999 is plotted. In **b**, the dotted region denotes temperature changes >15°C

Model minus GPCP  $P$  in each bin is displayed in the right column of Fig. 5 for each model and the ensemble mean of all 10 model composites. Contours denote differences in percentage of global coverage for each bin box (solid contours show where that regime has higher global representation in the model while dashed contours show where the model simulates a smaller global coverage than ERA interim). The largest differences occur in the highest  $\omega$  and  $T$  percentile bins (warm descending regime). The ensemble mean overestimates  $P$  in this regime by more than 40% with some models overestimating by more than 80% (e.g. CNRM and GISS). This regime samples primarily ocean regions covering only a small fraction of the global area and generally low precipitation totals ( $\leq 4$  mm/day) will reduce the absolute  $P$  error.

There is also a tendency for some models to underestimate  $P$  in the moderate  $T$  and lower  $\omega$  bins (moderately warm, ascending regime), in particular the IPSL model. Again, this is a regime of relatively low global coverage but affects both land and ocean grid boxes. The FGOALS model overestimates  $P$  in the coldest  $T$  bins by more than 80% relative to GPCP and other models. This is related to a highly unrealistic sea ice distribution with ice extending to the coast of Ireland in the north Atlantic, diagnosed by the 0°C isotherm (more discussion in Sect. 4). The GISS model underestimates  $P$  over strongly ascending grid-boxes and overestimates  $P$  over strongly descending grid boxes.

To investigate the model biases in  $P$  composites further, the relationship between  $P$  and  $\omega$  were analysed on the native latitude-longitude grids for the models and for GPCP and ERA Interim. Monthly mean  $P$  at each grid box was correlated with grid-box  $\omega$  and a linear least squares fit computed,  $dP/d\omega$ . This was conducted separately for each of the four seasons over the period 1989–1999 (so 33 monthly means for each season and each grid box). The results are presented as an average of all four seasons in Fig. 6 for the GISS model, an average of the remaining 20C3 model simulations and GPCP/ERA Interim observations.

Over the tropics there is a negative relationship between  $P$  and  $\omega$  as expected (more negative  $\omega$  denotes stronger ascending vertical motion and increased precipitation). The GISS model displays a substantially different relationship between  $P$  and  $\omega$  compared to the remaining models and so we consider this model separately in Fig. 6a and an average of the remaining models in Fig. 6b. The GISS model simulations show a negative  $dP/d\omega \sim -40$  mm/day per Pa/s over many tropical grid points with relatively little relationship elsewhere apart from the Himalayas where  $\omega$  fields at 500 hPa were invalid or missing due to orography. For the remaining models tropical  $dP/d\omega$  is  $-100$  mm/day per Pa/s or more negative still over the tropical warm pool while weaker negative relationships of around  $-40$  mm/day per Pa/s are found over most other regions apart from

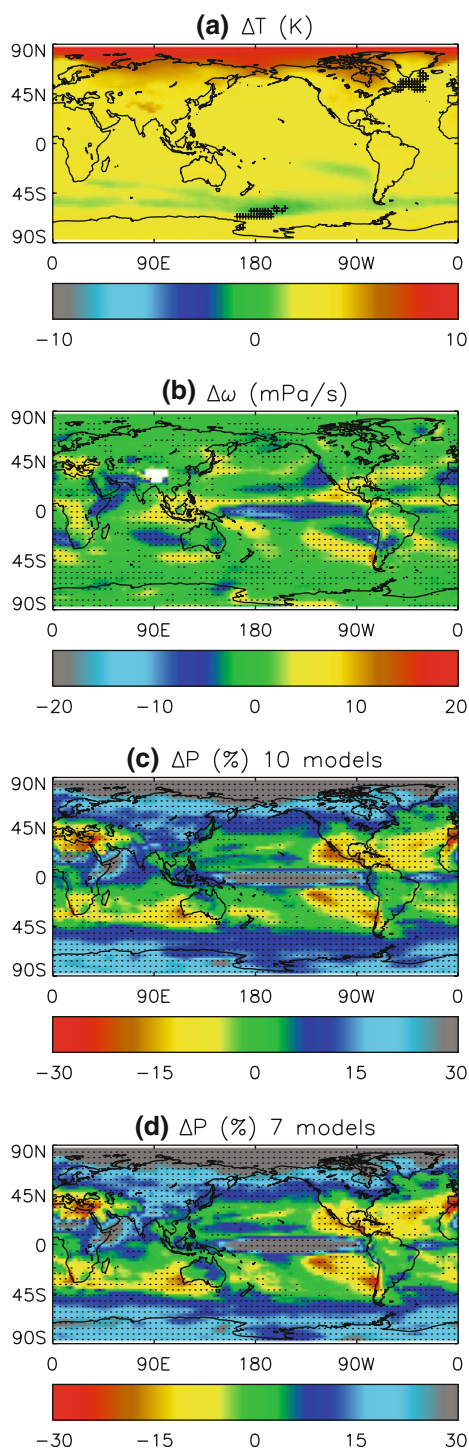


**Fig. 8** Ten-member ensemble-mean changes in annual mean (a) surface temperature (*crosses* denote where not all models agree on the sign of the change), (b) vertical motion at 500 hPa and (c) precipitation for 2080–2099 minus 1980–1999 (*dots* in b and c denote where at least 8 models agree on the sign of the change in b and c). Also shown (d) is the seven member ensemble mean (excluding GISS, FGOALS and IPSL models) change in precipitation; *dots* show where at least 6 out of the 7 models agree in the sign of the change (in b–d, *dots* are plotted for every 2nd grid box to improve clarity)

the poles and the dry subtropical regimes. Over these dry regions, changes in 500 hPa vertical motion have little effect on precipitation which is primarily determined by shallow cloud processes. The model distribution of mean  $dP/d\omega$  shows consistency with the GPCP-ERA Interim observational estimate in Fig. 6c suggesting that the GISS model diagnostics are unrealistic and may generate spurious  $P$  composites and their variation.

#### 4 Projected changes in precipitation, surface temperature and vertical motion

Changes in annual mean  $P$ ,  $T$  and  $\omega$  are now considered for the period 2080–2099 minus 1980–1999 using climate change simulations from the SRES A1B scenario and present day simulations from the 20C3 experiments. There are a variety of seasonal responses simulated by each model (not shown); changes in seasonal  $T$  are particularly extreme in two models (FGOALS and IPSL). Fig. 7 shows 100 year changes in  $T$  for March to May (MAM; top) and September–November (SON; bottom) for the FGOALS model (left), IPSL (middle) and an ensemble of the remaining 8 models (right).

The Arctic ocean is subject to a substantial rise in  $T$ , in excess of 8 K for SON for the model ensemble (Fig. 7f) related partly to the melting of Arctic sea ice. This area of rapidly rising ocean temperatures surrounding the Arctic ocean (north Atlantic and north Pacific) is substantially larger in the FGOALS simulation: the 0°C isotherm for 1980–1999 (contour in Fig. 7) extends as far south as Ireland, symptomatic of highly unrealistic sea ice extent. The melting of this unrealistic sea ice in the north Pacific and north Atlantic lead to rises in  $T$  greater than 4 K during MAM and more than 8 K in the north Atlantic during SON in the FGOALS model. These rises in  $T$  do not appear to be associated with unusual changes in  $P$  relative to the remaining models however.

Rises in  $T$  over northern high latitude spring are largest in the IPSL model simulations, in particular over the continents, with increases reaching above 15°C over Siberia (Fig. 7b). The rapid increases in  $T$  are also apparent over Antarctica and Australia during SON (Fig. 7e). Conversely rapid reductions in  $T$  over Eurasia in SON (reductions of  $-4^{\circ}\text{C}$  and below over Siberia, Fig. 7e) are at odds with the remaining models (Fig. 7f). These substantial changes in continental  $T$  simulated by the IPSL model are also associated with increases in  $P$  greater than 30% in MAM and declining  $P$  during SON over Siberia (not shown).

Fig. 8 summarises the 100 year 10-model ensemble mean changes in  $P$ ,  $T$  and  $\omega$ . There are widespread increases in  $P$  poleward of 45° in latitude and over

equatorial regions but reduced  $P$  (Fig. 8c) over subtropical dry regions, despite the more uniform global increases in  $T$  (Fig. 8a), consistent with previous analysis (Meehl et al. 2007a; Held and Soden 2006). 73% of the global surface area experiences a consistent sign of change in  $P$  in at least 8 out of 10 models. Some of the  $P$  responses are associated with circulation changes diagnosed by 500 hPa  $\omega$  in Fig. 8b, consistent with the relationships between  $P$  and  $\omega$  demonstrated in Figs. 1 and 6; the climate change responses are analysed in more detail by Chou et al. (2009). However, previous discussions (Meehl et al. 2007a) note that the sign of the changes in  $P$  are uncertain over many subtropical regions with substantial disagreement amongst models. Considering the unusual behaviour of the IPSL and FGOALS models in simulating projected  $T$  responses (Fig. 7) and the unrealistic relationship between  $P$  and  $\omega$  simulated by the GISS model (Fig. 6) a 7-member ensemble of the remaining climate models is also considered in Fig. 8d. This shows a similar structure of change to the 10-member ensemble; 54% of the global area exhibits a consistent sign of grid-point changes in  $P$  in at least 6 out of the 7 models considered as denoted by the dotted region in Fig. 8d.

The regional  $P$  response is also particularly sensitive to the mean and seasonal location of the large-scale circulation and so climatological biases may impact the reliability of each model climate projection. This motivates the use of the compositing techniques developed in the previous sections to further analyse changes in  $P$ .

## 5 Projected changes in precipitation composites

Changes in  $P$  are now considered as a function of dynamical regime using the  $T$  and  $\omega$  composites. Multi-annual mean global  $P$  composites were generated for the periods 1980–1999 and 2080–2099 for each model. Figure 9 shows the 2080–2099 minus 1980–1999 percentage change in  $P$  for each  $T$  and  $\omega$  percentile bin box normalised by the  $T$  change (%/K). Also shown is the mean change in  $\omega$  for each percentile bin of  $\omega$ .

Over most  $T$  percentiles,  $T$  rises range from nearly 2K (MRI CGCM model) up to 4K for the MIROC high resolution model (not shown). Changes in  $P$  composites show consistent patterns across the models (Fig. 9) with increases for the colder  $T$  percentiles ( $\sim 4\%/K$ ) and also for the the lower (ascending)  $\omega$  percentiles. Decreases in  $P$  primarily affect the higher  $T$  and  $\omega$  percentiles (warm, descent). There is also a tendency for a shift in the distribution from the warmest, strongest descent bins to lower  $T$  percentiles in some models (e.g. MIROC) as denoted by an increase in the percentage area coverage (solid contours).

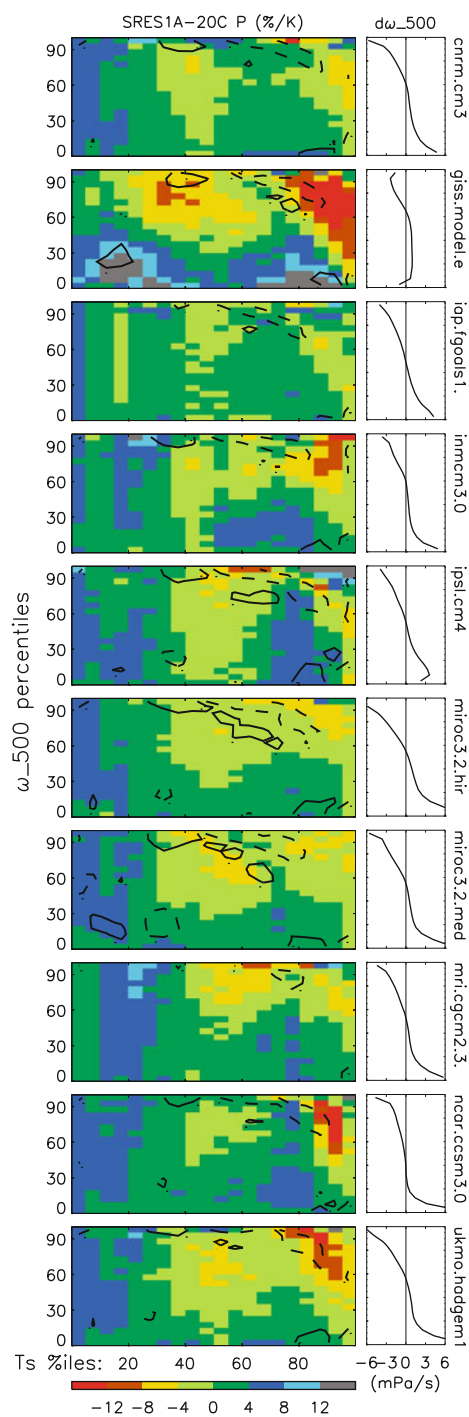


**Fig. 9** 2080–2099 SRES A1B minus 1980–1999 20C3 changes in (left) precipitation in bins of temperature and vertical motion (solid contours denote 0.05% increases and dashed contours 0.05% decreases in global area coverage of each bin) and (right) vertical motion changes as a function of vertical motion percentiles

The distribution of  $\omega$  also alters with ascent and descent on average becoming weaker, associated in part with a weakening Walker circulation (Vecchi et al. 2006). On its own, this would act to reduce  $P$  in the ascending regimes;

this is not the case since increases in low level moisture determined by the Clausius Clapeyron equation maintain a rise in  $P$  (Held and Soden 2006) for all models over most of the lowest  $\omega$  bins (strongest ascent). The GISS-E-R model exhibits the smallest change in the  $\omega$  distribution and the largest changes in  $P$ , more than 12%/K increases over ascending regimes and less than -12%/K for the warmest descending regimes. This response is likely to be affected by the unrealistic  $P - \omega$  relationship in the tropics simulated by this model (Fig. 6).

Multi-model ensemble mean composites of  $P$  and their response are displayed in Fig. 10 for all grid-points, ocean-only points and land-only points. For the 10 climate models (Table 1) considered in the ensemble there is broad consistency in the  $T$  and  $\omega$  responses between land and ocean with polar amplification in temperature changes and a weakening of the mean upward and downward vertical motion. Increases in  $P$  with warming are particularly marked for the lowest  $T$  percentiles over land and for warm ascending ocean regions (60–80th  $T$  percentile and 0–30th  $\omega$  percentiles) where  $dP/dT$  is generally greater than 4%/K. Negative  $dP/dT$  for warm, high  $\omega$  percentiles (descent) is strongest for the mid-range  $T$  percentiles and highest  $T$  percentiles over ocean but around the 60–80th  $T$  percentiles over land.

Where  $dP/dT$  is of the same sign in at least 8 out of 10 of the models considered a dot is displayed (Fig. 10c). Above 70% of grid points, weighted by area, experience a consistent sign of change in  $dP/dT$ . The consistency amongst models is lower over descending land bins (around 60% of the global land area experiences a consistent sign of change

in at least 8 of the 10 models). The FGOALS and NCAR CCSM models simulate positive  $dP/dT$  over most land regions, regardless of  $T$  and  $\omega$  percentile while the IPSL model displays  $dP/dT > 8\%/K$  for the warmest land  $T$  percentiles and  $dP/dT < -4\%/K$  for moderate  $T$  percentiles (not shown). The consistency in  $P$  response over warm, descending regimes over land is increased somewhat when the GISS, FGOALS and IPSL models were excluded from the ensemble based upon the unrealistic simulations and responses discussed in previous sections (Fig 11). For the reduced ensemble the global area experiencing a consistent sign of change in  $dP/dT$  is 69%, larger than the corresponding consistency from Fig. 8d.

Finally, the influence of the changes in vertical motion on the  $P$  responses are assessed. To achieve this, the sensitivity of  $P$  to changes in  $\omega$  are estimated in each  $T$  percentile:

$$\frac{\partial P}{\partial \omega} \sim \left. \frac{dP}{d\omega} \right|_T \quad (1)$$

This is computed by applying a centred finite difference at each bin box, apart from the strongest ascent and strongest descent percentile rows.  $\partial P/\partial \omega$  is estimated for the 1980–1999 and 2080–2099 ensemble mean  $P$  distributions and the average is displayed in Fig. 12a. This is comparable to the sensitivity calculated in longitude-latitude space in Fig. 6, ranging from close to zero up to -120 mm/day per Pa/s for the warmest, ascending regimes. The computed sensitivity is multiplied by the changes in  $\omega$  from 1980–1999 to 2080–2099 for each bin box:

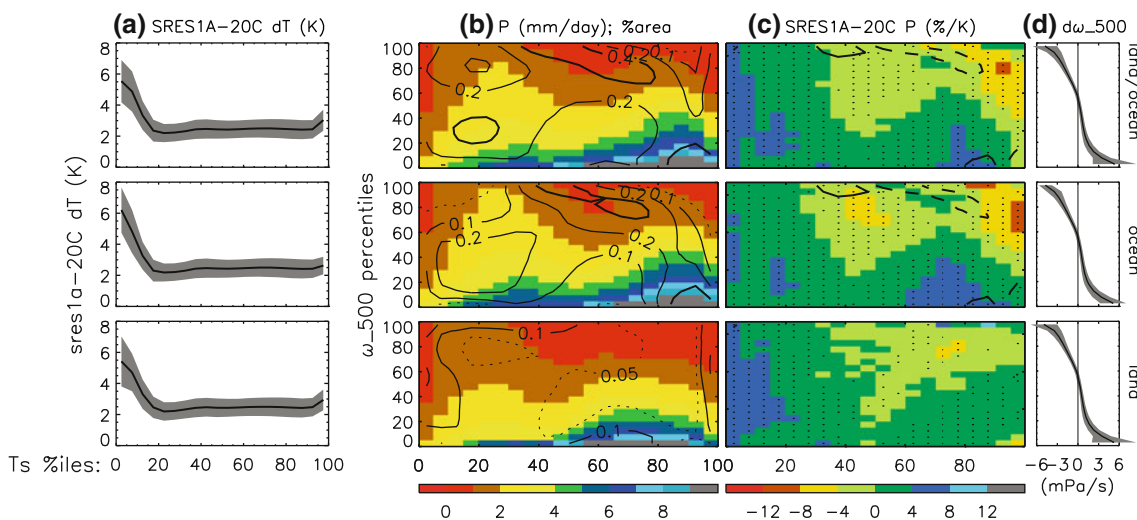


**Fig. 10** Model ensemble mean (a) changes (2080–2099 minus 1980–1999) in temperature, (b) 2080–2099 mean precipitation with contours showing percentage of global area sampled for each bin box (contours at 0.05% (dotted), 0.1, 0.2 and 0.4% (bold)) and 2080–2099 minus 1980–1999 changes in (c) precipitation (%/K) and (d) vertical

motion at 500 hPa, for all (top), ocean-only (middle) and land-only (bottom). In (c), solid/dashed contours denote increased/decreased fractional coverage and dots show where at least 8 out of 10 models agree on the sign of precipitation change

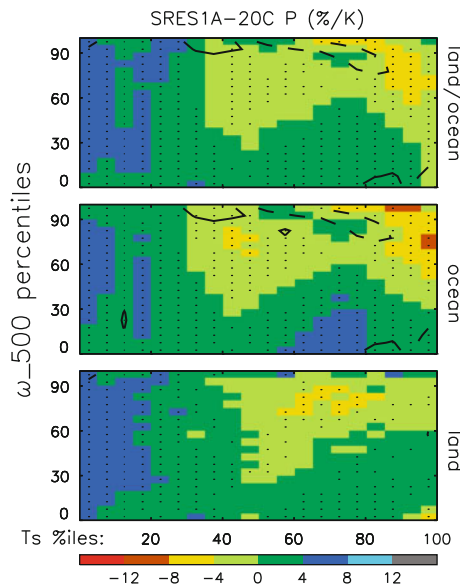


**Fig. 11** Model ensemble mean (excluding GISS, FGOALS and IPSL models) 2080–2099 minus 1980–1999 changes in precipitation (%/K) for all (top), ocean-only (middle) and land-only (bottom). Contours denote changes in fractional coverage and dots show where at least 6 out of 7 models agree on the sign of precipitation change

$$\Delta P(\Delta\omega) = \frac{\partial P}{\partial \omega} \Delta\omega. \quad (2)$$

The resulting  $\Delta P(\Delta\omega)$  is displayed in Fig. 12b and demonstrates that the changes in  $\omega$  contribute a decline of 6% in  $P$  in the warm, ascending regime and a rise in  $P$  of similar magnitude in the warm, descending regime. These changes are subsequently removed from the ensemble mean changes in  $P$  such that  $dP/dT$  independent of changes in  $\omega$  can be estimated (Fig. 12c). Comparing with Fig. 10c (top) demonstrates that the reduction in the strength of the Walker circulation in models, discussed previously (e.g. Held and Soden 2006), reduces the contrasting  $dP/dT$  in the wet and dry regions of the tropics only marginally. The  $P$  changes independent of  $\omega$  changes range from  $-12\%/K$  in the warmest, descending branch of the tropical circulation up to  $+7\%/K$  in the warm ( $\sim 80$ th  $T$  percentile) ascending branch of the tropical circulation.

## 6 Conclusions

A technique is presented to enable the assessment of changes in precipitation ( $P$ ) as a function of percentiles of surface temperature ( $T$ ) and 500 hPa vertical pressure velocity ( $\omega$ ). This allows changes in  $P$  composites to be considered in terms of dynamical regime rather than for fixed geographic regions, aiding the interpretation in terms of the driving process-based physical mechanisms.

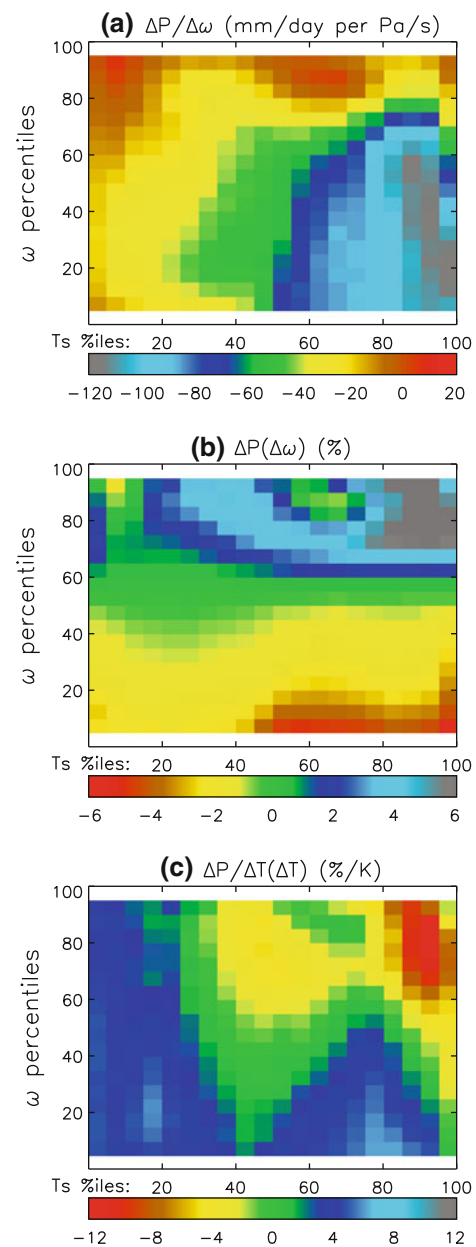


**Fig. 12** Estimated precipitation response with the signal related to changes in vertical motion removed: (a) calculated sensitivity  $dP/d\omega$  as a function of percentile bins of  $\omega$  and  $T$  based upon the 1980–1999 and 2080–2099 model ensemble mean  $P$  distributions; (b) the estimated 2080–2099 minus 1980–1999 precipitation change due to changes in  $\omega$  in each percentile bin and (c) the calculated  $dP/d\omega$  with the  $dP(d\omega)$  signal removed

Considering climate change projections between 1980–1999 and 2080–2099, a distinct pattern of  $P$  change is determined. The primary responses are  $dP/dT \geq 4\%/K$  over the coldest land points and warm, ascending ocean points. However,  $P$  generally declines over warm, descending regimes. This is consistent with theoretical constraints involving enhanced moisture fluxes between low and high latitudes and from dry to moist tropical

regions (Held and Soden 2006), although the tropical signal is diminished somewhat by a reduction in the strength of the Walker circulation (Vecchi et al. 2006). Considering the  $P$  distributions as a function of  $\omega$  it is found that the declining Walker circulation reduces model ensemble mean  $P$  in the warmest, ascending regimes by  $\sim 6\%$  and increases  $P$  in the tropical descending regimes by up to  $6\%$ . Removing this effect results in a clearer signal of contrasting  $P$  responses in the wet and dry tropical regimes.

The contrasting wet and dry regime  $P$  responses also appear consistent with limited observational evidence over tropical oceans (Allan et al. 2010); it is planned in future work to analyse in more detail the present day variability and changes in observed and model  $P$  composites using this technique considering the latest CMIP5 models over the present day and over the next few decades and utilising new, extended global observational datasets (Arkin et al. 2010). It is important also to note that over decadal timescales the Walker circulation may temporarily strengthen (Vecchi et al. 2006; Sohn and Park 2010; Zahn and Allan 2011) with implications for decadal changes in precipitation.

While all the models considered indicate a robust decline in the strength of the Walker circulation, this does not appear to influence extreme rainfall which is strongly constrained by the Clausius Clapeyron equation (e.g. Pall et al. 2007) but is subject to a substantial spread in responses in the tropics relating to changes in vertical motion within the rainfall events (O’Gorman and Schneider 2009; Sugiyama et al 2010; Allan et al. 2010). Indeed, analysing monthly fields is not adequate for correctly sampling meteorological regimes which may require analysis of daily fields. A further application of the compositing technique may be in partitioning changes in daily to monthly  $P$  (and in other variables such as clouds and radiation) between thermodynamic and dynamic changes (Emori and Brown 2005; Bony et al. 2004) and for reducing the influence of unrealistic present-day simulations of the atmospheric circulation in climate model projections. It will also be important to characterise more carefully the consistency in the magnitude of precipitation changes, including regimes in which precipitation is unlikely to alter significantly (Ed Hawkins, pers. comm.).

**Acknowledgments** The modelling groups, the Programme for Climate Model Diagnosis and Intercomparison and the World Climate Research Programme’s Working Group on Coupled Modelling are acknowledged for their roles in making available the WCRP CMIP3 multi-model data set. Support of this data set is provided by the Office of Science, US Department of Energy. The Natural Environment Research Council are acknowledged for funding this work through the National Centre for Atmospheric Sciences (NCAS) Climate and the PREPARE project (NE/G015708/1). Matthias Zahn and two anonymous reviewers provided valuable comments on the manuscript.

## References

- Allan RP (2009) Examination of relationships between clear-sky longwave radiation and aspects of the atmospheric hydrological cycle in climate models, reanalyses, and observations. *J Clim* 22:3127–4145
- Allan RP, Soden BJ, John VO, Ingram I William, Good P (2010) Current changes in tropical precipitation. *Environ Res Lett* 5:025205. doi:10.1088/1748-9326/5/2/025205
- Allen MR, Ingram WJ (2002) Constraints on future changes in climate and the hydrologic cycle. *Nature* 419:224–232
- Andrews T, Forster PM, Boucher O, Bellouin N, Jones A (2010) Precipitation, radiative forcing and global temperature change. *Geophys Res Lett* 37:L14701. doi:10.1029/2010GL043991
- Arkin PA, Smith TM, Sapiano MRP, Janowiak J (2010) The observed sensitivity of the global hydrological cycle to changes in surface temperature. *Environ Res Lett* 5:035201. doi:10.1088/1748-9326/5/3/035201
- Bony S, Dufresne JL, Treut HL, Morcrette JJ, Senior C (2004) On dynamic and thermodynamic components of cloud changes. *Clim Dyn* 22:71–86
- Chou C, Tu J, Tan P (2007) Asymmetry of tropical precipitation change under global warming. *Geophys Res Lett* 34:L17708. doi:10.1029/2007GL030327
- Chou C, Neelin JD, and J-Y Tu CAC (2009) Evaluating the “rich get richer” mechanism in tropical precipitation change under global warming. *J Clim* 22:1982–2005
- Collins WD et al (2006) The community climate system model version 3 (CCSM3). *J Clim* 19:2122–2143
- Dee DP, Uppala SM, Simmons AJ, Berrisford P, Poli P, Kobayashi S, Andrae U, Balmaseda MA, Balsamo G, Bauer P, Bechtold P, Beljaars ACM, van de Berg L, Bidlot J, Bormann N, Delsol C, Dragani R, Fuentes M, Geer AJ, Haimberger L, Healy SB, Hersbach H, Hlm EV, Isaksen L, Killberg P, Khler M, Matricardi M, McNally AP, Monge-Sanz BM, Morcrette JJ, Park BK, Peubey C, de Rosnay P, Tavolato C, Thpaut JN, Vitart F (2011) The ERA-Interim reanalysis: configuration and performance of the data assimilation system. *Q J R Meteorol Soc* 137:553–597. doi:10.1002/qj.828
- Emori S, Brown SJ (2005) Dynamic and thermodynamic changes in mean and extreme precipitation under changed climate. *Geophys Res Lett* 32:L17706. doi:10.1029/2005GL023272
- Hasumi H, Emori S (2004) K-1 coupled model (MIROC) description. Tech. Rep. K-1 Tech. Rep. 1, Center for Climate System Research, University of Tokyo
- Held IM, Soden BJ (2006) Robust responses of the hydrological cycle to global warming. *J Clim* 19:5686–5699
- Huffman GJ, Adler RF, Bolvin DT, Gu G (2009) Improving the global precipitation record: GPCP version 2.1. *Geophys Res Lett* 36:L17808. doi:10.1029/2009GL040,000
- Johns TC, Durman CF, Banks HT, Roberts MJ, McLaren AJ, Ridley JK, Senior CA, Williams KD, Jones A, Rickard GJ, Cusack S, Ingram WJ, Crucifix M, Sexton DMH, Joshi MM, Dong BW, Spencer H, Hill RSR, Gregory JM, Keen AB, Pardaens AK, Lowe JA, Bodas-Salcedo A, Stark S, Searl Y (2006) The new Hadley Centre Climate Model (HadGEM1): Evaluation of coupled simulations. *J Climate* 19:1327–1353
- Lambert FH, Webb MJ (2008) Dependency of global mean precipitation on surface temperature. *Geophys Res Lett* 35:L16706. doi:10.1029/2008GL034838
- Marti O, Braconnot P, Bellier J, Benshila R, Bony S, Brockmann P, Cadulle P, Caubel A, Denvil S, Dufresne J, Fairhead L, Filiberti M, Fichefet T, Friedlingstein P, Grandpeix J, Hourdin F, Krinner G, Levy C, Musat I, Talandier C, The IPSL global climate modeling group (2005) The new IPSL climate system model:

- IPSL-CM4. Tech Rep Tech Rep no. 26, Institut Pierre Simon Laplace des Sciences de l'Environnement Global, IPSL, Case 101, Paris, France
- Meehl G, Stocker T, Collins W, Friedlingstein P, Gaye A, Gregory J, Kitoh A, Knutti R, Murphy J, Noda A, Raper S, Watterson I, Weaver A, Zhao ZC (2007a) Global climate projections, Cambridge University Press, Cambridge, pp 747–845. Climate Change 2007: The physical science basis. Contribution of working group I to the fourth assessment report of the intergovernmental panel on climate change
- Meehl GA, Covey C, Delworth T, Latif M, McAvaney B, Mitchell JFB, Stouffer RJ, Taylor KE (2007) The WCRP CMIP3 multimodel dataset: a new era in climate change research. *Bull Amer Met Soc* 88:1383–1394
- Mitchell J, Wilson CA, Cunningham WM (1987) On CO<sub>2</sub> climate sensitivity and model dependence of results. *Q J R Meteorol Soc* 113:293–322
- O’Gorman PA, Muller CJ (2010) How closely do changes in surface and column water vapor follow Clausius-Clapeyron scaling in climate change simulations. *Environ Res Lett* 5:025207. doi: [10.1088/1748-9326/5/2/025207](https://doi.org/10.1088/1748-9326/5/2/025207)
- O’Gorman PA, Schneider T (2009) The physical basis for increases in precipitation extremes in simulations of 21st-century climate change. *Proc Nat Acad Sci* 106:14,773–14,777
- Pal JS, Giorgi F, Bi X (2004) Consistency of recent european summer precipitation trends and extremes with future regional climate projections. *Geophys Res Lett* 31(13):L13202. doi: [10.1029/2004GL019836](https://doi.org/10.1029/2004GL019836)
- Pall P, Allen MR, Stone DA (2007) Testing the clausius clapeyron constraint on changes in extreme precipitation under CO<sub>2</sub> warming. *Clim Dyn* 28:351–363
- Salas-Mélia D, Chauvin F, Déqué M, Douville H, Guérémy J, Marquet P, Planton S, Royer J, Tyteca S (2005) Description and validation of the CNRM-CM3 global coupled model. Technical Report CNRM working note 103, Météo-France, 42 Avenue Gaspard Coriolis, 31057 Toulouse Cedex, France
- Schmidt GA, co-oauthors (2006) Present-day atmospheric simulations using GISS ModelE: comparison to in situ, satellite, and reanalysis data. *J Clim* 19:153–192
- Sohn BJ, Park SC (2010) Strengthened tropical circulations in past three decades inferred from water vapor transport. *J Geophys Res* 115:D15112. doi: [10.1029/2009JD013713](https://doi.org/10.1029/2009JD013713)
- Stephens GL, Ellis TD (2008) Controls of global-mean precipitation increases in global warming GCM experiments. *J Clim* 21:6141–6155
- Sugiyama M, Shiogama H, Emori S (2010) Precipitation extreme changes exceeding moisture content increases in MIROC and IPCC climate models. *Proc Nat Acad Sci* 107:571–575
- Trenberth KE, Shea DJ (2005) Relationships between precipitation and surface temperature. *Geophys Res Lett* 32(14):L14703. doi: [10.1029/2005GL022760](https://doi.org/10.1029/2005GL022760)
- Trenberth KE, Dai A, Rasmussen RM, Parsons DB (2003) The changing character of precipitation. *Bull Amer Met Soc* 84:1205–1217
- Vecchi GA, Soden BJ, Wittenberg AT, Held IM, Leetmaa A, Harrison MJ (2006) Weakening of tropical pacific atmospheric circulation due to anthropogenic forcing. *Nature* 441:73–76
- Volodin EM, Diansky NA (2004) El Niño reproduction in coupled general circulation model. *Russ Meteor Hydrol* 12:5–14
- Willett KM, Jones PD, Gillett NP, Thorne PW (2008) Recent changes in surface humidity: development of the HadCRUH dataset. *J Clim* 21(20):5364–5383
- Williams J, Ringer MA (2010) Precipitation changes within dynamical regimes in a perturbed climate. *Environ Res Lett* 5:035202. doi: [10.1088/1748-9326/5/3/035202](https://doi.org/10.1088/1748-9326/5/3/035202)
- Xie SP, Deser C, Vecchi G, Ma J, Teng H, Wittenberg A (2010) Global warming pattern formation: Sea surface temperature and rainfall. *J Clim* 23:966–986
- Yu Y, Zhang Z, Guo Y (2004) Global coupled ocean-atmosphere general circulation models in LASG/IAP. *Adv Atmos Sci* 21: 444–455
- Yukimoto S, Noda A (2002) Improvements in the Meteorological Research Institute Global Ocean-Atmosphere Coupled GCM (MRI-CGCM2) and its climate sensitivity. Tech Rep Tech Rep 10, NIES, Japan
- Zahn M, Allan RP (2011) Changes in water vapor transports of the ascending branch of the tropical circulation. *J Geophys Res* (submitted)